Thermodynamics of a minimal interacting heat engine: Comparison between engine designs

Thermodynamics of a minimal interacting heat engine: Comparison between engine designs

Felipe Hawthorne,[1] B. Cleuren,[2] and Carlos E. Fiore[1]

[1]*Universidade de São Paulo, Instituto de Física, Rua do Matão, 1371, 05508-090 São Paulo, SP, Brazil*
[2]*UHasselt, Faculty of Sciences, Theory Lab, Agoralaan, 3590 Diepenbeek, Belgium*

(Dated: June 13, 2024)

Collective effects stemming from many interacting units have attracted remarkable recent interest, not only for their presence in several systems in nature but also for the possibility of being used for the construction of efficient engine setups. Notwithstanding, little is known about the influence of the engine design, and most studies are restricted to the simplest cases (e.g. simultaneous contact with two thermal baths), not necessarily constituting a realistic setup implementation. In order to investigate the design and its influence on the performance, we introduce the collisional/sequential description for a minimal model for interacting heat engines, composed of two coupled nanomachines placed in contact with a distinct thermal reservoir and subjected to a nonequilibrium worksource at each stage. Thermodynamic quantities are exactly obtained irrespectively the model details. Distinct kinds of worksources are investigated and the influence of the interaction, temperature, period, and time asymmetry has been undertaken. Results show that a careful design of interaction provides superior performance than the interactionless case, including optimal power outputs and efficiencies at maximum power greater than known bounds or even the system presenting efficiencies close to the ideal (Carnot) limit. As a complementary analysis, we also show that the case of the system simultaneously placed in contact with two thermal reservoirs constitutes a particular case of our framework.

I. INTRODUCTION

The construction of nanoscopic steady-state heat engines has attracted a great deal of recent attention in the realm of stochastic thermodynamics [1–5], not only for extending the fundamental concept of the energy conversion (from the macroscopic to the nanoscopic scale), but also because it presents three fundamental differences when compared with the equilibrium thermodynamics. First, there is no need for moving parts and pistons since the energy conversion comes from currents of microscopic particles/units. Second, nanoscopic-engineered setups typically operate far from equilibrium and consequently, its performance is expected to be lower than the ideal case. Third, fluctuations of quantities and currents can become important in small-scale systems. The issues above illustrate the search for the optimal protocol as crucial to ensure its reliability and desired performance.

In the last years, distinct kinds of engines operating far from equilibrium have been proposed and investigated [1, 6–10]. Under a generic point of view, they are grouped out in three categories, stemming from fixed thermodynamic forces [11–17], from the time-periodic variation of external parameters [18–21] and via sequential/collisional approach [22–27], in which at each stage, the system is subjected to a different condition (held fixed along the stage). Each one has been considered as a reliable approach in distinct contexts, the latter encompassing the presence of distinct drivings over each member of the system, a weak coupling between the system with the reservoir, or even for mimicking the environment for quantum systems. While most of the above studies are restricted to setups composed of one unit [19, 20, 24, 25, 28], the thermodynamics of systems exhibiting collective effects and/or those composed of interacting units has received considerable recent attention as an alternative strategy for improving the system performance for quantum systems [29–48] and classical ones, such as interacting Brownian particles [21], work-to-work transducers [49, 50] and heat engines [16, 17]. All of them are restricted to cases of systems operating at equal temperatures [49, 50], fixed parameters [16, 17] or sinusoidal drivings [21].

In this contribution, we conciliate the points above by investigating a minimal model for collective effects, formed by two interacting units placed sequentially in contact with distinct thermal baths at each stage. Previous studies have tackled different versions, such as its all-to-all (mean-field) design [16, 17] and distinct topology of interactions [15], all of them restricted to the case of fixed thermodynamic forces and a large number of units. Our study will focus on the opposite case, dealing with a minimal collective effect system composed of two interacting units beyond the fixed forces context. Hence, its simplicity constitutes an ideal laboratory for comparing three fundamental aspects of nanoscopic engines: the kind of design (sequential versus fixed thermodynamic forces), distinct approaches for the worksource (not considered previously), and under situations collective effects can improve the system performance when compared with its interactionless version. The former goal has been inspired by previous contributions [25, 28], whereas the different worksources addressed here were considered in Refs. [15–17, 25]. It is worth mentioning that our system shares some similarities with recent studies about a setup composed of two interacting quantum dots under repeated interactions [51, 52]. Our findings reveal that the interaction between units, together with a suited design of parameters (energy, period, duration of each stage), can significantly enhance the system's performance. Such remarkable improvement can result in optimal power outputs, efficiencies at maximum power greater than known bounds, or even efficiencies approaching the ideal (Carnot) limit. Our minimal model already captures the essential features of the system, including the interplay between parameters, maximizations of power, and efficiency [15, 16]. As a side result, our study shows the simultaneous contact with two thermal baths case [16] as the ideal limit of fast switching times.

This paper is organized as follows. In Sec. II the model and the main expressions for thermodynamic quantities will be presented. In Secs. III and IV we shall analyze in detail two distinct approaches for our engine setup. Conclusions will be drawn in Sec. V.

II. MODEL AND THERMODYNAMICS

Our minimal model for collective effects is composed of two interacting units sequentially placed into contact with N distinct reservoirs, each one of duration $\tau_\nu - \tau_{\nu-1}$, with $\nu = 1, ..., N$ and $\tau_0 = 0$. The total time to complete one cycle being τ. At each stage, occurring between $\tau_{\nu-1} < t \leq \tau_\nu$, each unit can be in a lower ($\sigma_k = 0$) or upper ($\sigma_k = 1$) state, with individual energies 0 and ϵ_ν, respectively. The system is connected to the reservoir ν, with temperature $\beta_\nu = 1/(k_B T_\nu)$, whose total energy is given by the sum of individual and interaction components:

$$\tilde{\epsilon}^{(\nu)} = V_\nu[(1-\sigma_1)\sigma_2+\sigma_1(1-\sigma_2)]+U_\nu\sigma_1\sigma_2+\epsilon_\nu(\sigma_1+\sigma_2), \quad (1)$$

where U_ν, V_ν correspond to distinct interaction energies, provided they are in the same and different states, respectively. Throughout this paper, we adopt $k_B = 1$. In addition, the system can be subjected to a non-conservative force.

After the time duration τ_ν, it is disconnected and reconnected to the next reservoir with temperature $\beta_{\nu+1} = 1/T_{\nu+1}$ and subjected to another set of parameters $\epsilon_{\nu+1}$, $U_{\nu+1}$, $V_{\nu+1}$ and $F_{\nu+1}$. This process is then repeated until a complete cycle, after the total time τ. Collisional description usually neglects the time for changing the contact between the system and thermal baths and for this reason, we have not considered the difference of energy due to the change of the stage. We shall assume throughout this paper that τ is large enough for the collisional approximation to be valid, in such a way that the difference of energy required for changing the stage is neglected. As in Refs. [15, 16, 53], the above system dynamics becomes simpler when characterized by the total particle number i occupying the upper state, assuming the values $i = 0, 1$ or 2, according to whether it is empty, having one unit, or having two units, with energies $\tilde{\epsilon}^{(\nu)} = 0, V_\nu + \epsilon_\nu$ and $U_\nu + 2\epsilon_\nu$, respectively. Let $p_i^{(\nu)}(t)$ be the system's probability at the state i at the time t when it is placed in contact with the ν-th reservoir, governed by the following master equation

$$\dot{p}_i^{(\nu)}(t) = \sum_{j\neq i} J_{ij}^{(\nu)}, \quad (2)$$

where $p_i^{(1)}(t)$ and $p_i^{(2}(t)$ describes the system behavior during $0 \leq t < \tau_1$ and $\tau_1 \leq t < \tau$, respectively, and $J_{ij}^{(\nu)} \equiv \omega_{ij}^{(\nu)} p_j^{(\nu)} - \omega_{ji}^{(\nu)} p_i^{(\nu)}$ and $\omega_{ij}^{(\nu)}$ accounts to the transition rate from state j to i, satisfying the condition $\sum_i \omega_{ij}^{(\nu)} = 0$ for every stages.

We shall restrict our analysis to the simplest case $N = 2$, as sketched in Fig. 1, in which the time duration of the first and second stages read τ_1 and $\tau_2 = \tau - \tau_1$, respectively. Note that one has the symmetric time operation when $\tau_1 = \tau/2$. Given that the probability distribution is continuous in time,

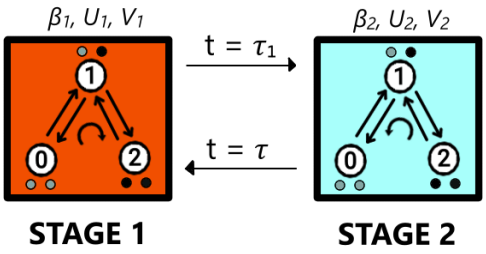

FIG. 1. Sketch of the present setup characterized by a three-state system specified by the variable i accounting to the occupation of the upper level. At each stage, specified by distinct colors, the system can assume distinct values of energy parameters and be subject to a biased force (see e.g. main text). The stage change occurs at $t = \tau_1$ and the system returns to its initial state at $t = \tau$.

it should satisfy the following boundary conditions for $p_i^{(\nu)}(t)$ (for all $i = 0, 1$ and 2):

$$p_i^{(1)}(\tau_1) = p_i^{(2)}(\tau_1), \qquad p_i^{(1)}(0) = p_i^{(2)}(\tau). \quad (3)$$

The probability flux in the right side of Eq. (2) can also be expressed in terms of the evolution matrix, $W^{(\nu)}$, that, in turn, can be written in terms of the transition rates,

$$W^{(\nu)} = \begin{pmatrix} -\omega_{10}^{(\nu)} & \omega_{01}^{(\nu)} & 0 \\ \omega_{10}^{(\nu)} & -\omega_{01}^{(\nu)} - \omega_{21}^{(\nu)} & \omega_{12}^{(\nu)} \\ 0 & \omega_{21}^{(\nu)} & -\omega_{12}^{(\nu)} \end{pmatrix},$$

whose largest eigenvalue, $\lambda_0 = 0$, has its associated left and right eigenvalues given by

$$\left|\psi_0^{(\nu)}\right\rangle \equiv \left|p^{(eq,\nu)}\right\rangle = \begin{pmatrix} p_0^{(eq,\nu)} \\ p_1^{(eq,\nu)} \\ 1 - p_0^{(eq,\nu)} - p_1^{(eq,\nu)} \end{pmatrix}$$

and $\left\langle\phi_0^{(\nu)}\right| = (111)$, respectively, whereas $\lambda_j^{(\nu)} < 0$ ($j > 0$) is the j-th non-zero eigenvalue, $\Gamma_j^{(\nu)} = \left|\psi_j^{(\nu)}\right\rangle\left\langle\phi_j^{(\nu)}\right|$ is the matrix associated with the product of the j-th right and left eigenvectors and the normalization property of eigenvectors implies that $\left\langle\phi_i^{(\nu)}\middle|\psi_j^{(\nu)}\right\rangle = \delta_{ij}$. By resorting to the eigendecomposition of Eq. (2), along with the periodic boundary conditions given by Eq. (3), it is possible to obtain the expression for the probability vector $\left|p_i^{(\nu)}(t)\right\rangle$ at the ν-th stage:

$$\left|p^{(\nu)}(t)\right\rangle = \left|p^{(eq,\nu)}\right\rangle + \sum_{j=1}^{2} e^{\lambda_j^{(\nu)}[t-\tau_{\nu-1}]}\Gamma_j^{(\nu)}\left|p^{(\nu)}(\tau_{\nu-1})\right\rangle, \quad (4)$$

where $\left|p^{(\nu)}(\tau_{\nu-1})\right\rangle$ is the probability vector obtained from the above boundary conditions and reads

$$\left|p^{(\nu)}(\tau_{\nu-1})\right\rangle = \begin{pmatrix} p_0^{(\nu)}(\tau_{\nu-1}) \\ p_1^{(\nu)}(\tau_{\nu-1}) \\ 1 - p_0^{(\nu)}(\tau_{\nu-1}) - p_1^{(\nu)}(\tau_{\nu-1}) \end{pmatrix}.$$

Despite being exact, expressions for $\left|p^{(\nu)}(\tau_{\nu-1})\right\rangle$ are quite cumbersome. In Appendix A, we list them for the particular case $\tau_1 = \tau/2$. Once the probability distribution is known, all thermodynamic quantities can be obtained. By integrating Eq. (2) over a complete cycle and subsequentially summing them, one has that $\sum_{j\neq i}\bar{J}^{(1)}_{ij} = -\sum_{j\neq i}\bar{J}^{(2)}_{ij}$, where $\overline{J}^{(1)}_{ij} = \int_0^{\tau_1} J^{(1)}_{ij}dt/\tau$, $\overline{J}^{(2)}_{ij} = \int_{\tau_1}^{\tau} J^{(2)}_{ij}dt/\tau$ and Eq. (3) was used. At each time, only transitions $i \to i \pm 1$ are allowed, implying that a transition of type $0 \leftrightarrow 2$ (both units occupying the lower and upper states, respectively) is forbidden and hence the system presents only two independent fluxes, namely $\bar{J}^{(1)}_{01}$ and $\bar{J}^{(1)}_{21}$, whose expressions are given by

$$\bar{J}^{(1)}_{01} = \frac{1}{\tau}\int_0^{\tau_1}\left\{\omega^{(1)}_{01}p^{(1)}_1(t) - \omega^{(1)}_{10}p^{(1)}_0(t)\right\}dt \tag{5a}$$

$$\bar{J}^{(1)}_{21} = \frac{1}{\tau}\int_0^{\tau_1}\left\{\omega^{(1)}_{21}p^{(1)}_1(t) - \omega^{(1)}_{12}p^{(1)}_2(t)\right\}dt, \tag{5b}$$

respectively. We pause to make a few comments about fluxes $\bar{J}^{(1)}_{ij}$'s. Firstly, for fast switchings $\tau \to 0$, each flux $\bar{J}^{(\nu)}_{ij}$ acquires a simpler form given by

$$\bar{J}^{(\nu)}_{ij} \to \frac{1}{2}\left\{\omega^{(\nu)}_{ij}p_j - \omega^{(\nu)}_{ji}p_i\right\}, \tag{6}$$

for $j = 1$ and $i \in \{0, 2\}$, where $p_i = p^{(1)}_i + p^{(2)}_i$, whose expressions are listed in Appendix B. Such limit is equivalent to the system being simultaneously placed in contact with both thermal baths. Secondly, in the regime of slow switchings, $\tau \gg 1$, fluxes $J^{(\nu)}_{10}$ and $J^{(\nu)}_{21}$ can be rewritten in the following form

$$J^{(\nu)}_{10} = (-1)^{(\nu+1)}\frac{p^{(eq,1)}_0 - p^{(eq,2)}_0}{\tau} \tag{7}$$

$$J^{(\nu)}_{21} = (-1)^{(\nu+1)}\frac{p^{(eq,1)}_2 - p^{(eq,2)}_2}{\tau} \tag{8}$$

which vanishes as $\tau \to \infty$, consistent with the case of the system being placed in contact with a single thermal reservoir.

Until here, all analyses have been carried out without any thermodynamic consideration. In order to introduce the relationship between energy exchanged and heat, we follow the approach commonly considered in the literature (see, *e.g.*, Refs. [1, 16, 17, 54, 55]) in which the ratio between transition rates $\omega^{(\nu)}_{ij}$ and $\omega^{(\nu)}_{ji}$ are defined according to the local detailed balance:

$$\ln\frac{\omega^{(\nu)}_{ij}}{\omega^{(\nu)}_{ji}} = -\beta_\nu\left[\tilde{\epsilon}^{(\nu)}_i - \tilde{\epsilon}^{(\nu)}_j + d^{(\nu)}_{ij}F_\nu\right], \tag{9}$$

where $\tilde{\epsilon}^{(\nu)}_i - \tilde{\epsilon}^{(\nu)}_j$ is the energy difference between states i and j and $d^{(\nu)}_{ji}F_\nu$ accounts to the influence of a driving force, where the element $d^{(\nu)}_{ji}$ is dimensionless scalar that has been introduced in order to describe the existence of a biased force, that satisfies the anti-symmetric property $d^{(\nu)}_{ji} = -d^{(\nu)}_{ij}$.

From Eq.(9) we consider the entropy production formula

$$\Pi_\nu(t) = \sum_{i<j} J^{(\nu)}_{ij}(t)\ln\frac{\omega^{(\nu)}_{ij}p_j(t)}{\omega^{(\nu)}_{ji}p_i(t)}, \tag{10}$$

whose integration over a complete cycle, together with the previously mentioned boundary conditions leads to the standard form $\bar{\sigma} = -\sum_\nu \beta_\nu \overline{\dot{Q}}_\nu$, where $\overline{\dot{Q}}_\nu$ is given by

$$\overline{\dot{Q}}_\nu = \sum_{i<j}\left[\tilde{\epsilon}^{(\nu)}_i - \tilde{\epsilon}^{(\nu)}_j + d^{(\nu)}_{ij}F_\nu\right]\overline{J}^{(\nu)}_{ij}. \tag{11}$$

By expressing Eq. (11) in terms of fluxes $\bar{J}^{(\nu)}_{01}$ and $\bar{J}^{(\nu)}_{21}$, the exchanged heat $\overline{\dot{Q}}_\nu$ then reads

$$\overline{\dot{Q}}_\nu = \left[\left(\tilde{\epsilon}^{(\nu)}_0 - \tilde{\epsilon}^{(\nu)}_1 + d^{(\nu)}_{01}F_\nu\right)\bar{J}^{(\nu)}_{01} + \left(\tilde{\epsilon}^{(\nu)}_2 - \tilde{\epsilon}^{(\nu)}_1 + d^{(\nu)}_{21}F_\nu\right)\bar{J}^{(\nu)}_{21}\right]. \tag{12}$$

Since the system evolves to a nonequilibrium steady state regime returning to the initial state after a complete cycle, the first law of thermodynamics establishes that the average power is given by $\mathcal{P} = -(\overline{\dot{Q}}_1 + \overline{\dot{Q}}_2)$, and hence, its expression reads

$$\mathcal{P} = -\left[\sum_i\left(\tilde{\epsilon}^{(2)}_i - \tilde{\epsilon}^{(1)}_i\right)\frac{\left(p^{(1)}_i(\tau_1) - p^{(1)}_i(0)\right)}{\tau} + \sum_{i<j} d^{(1)}_{ij}\left(F_1\overline{J}^{(1)}_{ij} - F_2\overline{J}^{(2)}_{ij}\right)\right], \tag{13}$$

where Eqs. (3) and (12) were used, together the properties: $d^{(1)}_{ij} = -d^{(2)}_{ij}$, $d^{(\nu)}_{ij} = -d^{(\nu)}_{ji}$ and $\overline{J}^{(\nu)}_{ij} = -\overline{J}^{(\nu)}_{ji}$. The above equation states that the power output comes from two work-sources: the former, from the time variation of energies (first term) after each stage and the latter from non-conservative forces (second term). By expressing in terms of independent fluxes, Eq. (13) reads $\mathcal{P} = \left[\left(\tilde{\epsilon}^{(2)}_0 - \tilde{\epsilon}^{(2)}_1\right) - \left(\tilde{\epsilon}^{(1)}_0 - \tilde{\epsilon}^{(1)}_1\right)\right]\bar{J}^{(1)}_{01} + \left[\left(\tilde{\epsilon}^{(2)}_2 - \tilde{\epsilon}^{(2)}_1\right) - \left(\tilde{\epsilon}^{(1)}_2 - \tilde{\epsilon}^{(1)}_1\right)\right]\bar{J}^{(1)}_{21} - \left(d^{(1)}_{01}\bar{J}^{(1)}_{01} + d^{(1)}_{21}\bar{J}^{(1)}_{21}\right)(F_1 + F_2)$.

Finally, by defining the second stage as the hot reservoir and choosing parameters properly, the amount of heat extracted from the hot bath $\overline{\dot{Q}}_2 > 0$ can be partially converted into power output $\mathcal{P} < 0$ ($\overline{\dot{Q}}_2 = -\mathcal{P} - \overline{\dot{Q}}_1$), consistent to the heat engine operation. Conversely, the pump regime is characterized by the amount of power required for delivering heat from the cold to the hot reservoir, implying that $\mathcal{P} = -\overline{\dot{Q}}_1 - \overline{\dot{Q}}_2$ with $\mathcal{P} > 0$ and $\overline{\dot{Q}}_2 < 0$. For characterizing both regimes, we adopt the efficiency definition $\eta = -\mathcal{P}/\overline{\dot{Q}}_2$, implying that the former and latter regimes have efficiencies constrained according to $0 \leq \eta < \eta_c$ and $\eta_c < \eta \leq \infty$, respectively, where $\eta_c = 1 - \beta_2/\beta_1$ denotes the Carnot efficiency. We stress that efficiencies greater than η_c in the latter case only mean that power is partly consumed for extracting heat from the hot to the cold bath, whose real performance is $1/\eta$. Conversely, when $\mathcal{P} > 0, \dot{Q}_2 > 0$, no energy conversion occurs, and the system operation is commonly referred to as in the *dud* regime, implying that $\eta < 0$ [16, 17, 21].

Despite the simplicity, the model presents a great number of parameters ($\beta_\nu, \epsilon_\nu, V_\nu, U_\nu, F_\nu$) and one of our main goals is to draw a comparison with previous results [16, 53] in which solely units in distinct states interact with each other. For this reason, we shall curb ourselves to the case $U_\nu = 0$.

III. DISTINCT INTERACTIONS AT EACH STAGE

Inspired in previous works [25, 26], our first approach consists of building a setup via change of individual and interaction energies at each stage without non-conservative drivings. In order to draw a comparison with the previous, the main features of the interactionless case will be depicted in the next section.

A. Interactionless case

For the interactionless case, transition rates are defined in the following form:

$$\omega_{10}^{(\nu)} = \Gamma \exp\left\{\frac{-\beta_\nu \epsilon_\nu}{2}\right\}, \qquad \omega_{01}^{(\nu)} = \Gamma \exp\left\{\frac{\beta_\nu \epsilon_\nu}{2}\right\}. \tag{14}$$

From Eqs. (2) and (13) for $F_1 = F_2 = 0$, the system power $\mathcal{P}_s$ is given by $\mathcal{P}_s = (\epsilon_1 - \epsilon_2)\bar{J}_s$ where, for $\tau_1 = \tau/2$, $\bar{J}_s$ reads:

$$\bar{J}_s = \frac{\prod_\mu \left\{-1 + \cosh\left[\tau \cosh\left(\frac{\beta_\mu \epsilon_\mu}{2}\right)\right] + \sinh\left[\tau \cosh\left(\frac{\beta_\mu \epsilon_\mu}{2}\right)\right]\right\}}{\left(e^{\beta_1\epsilon_1} - e^{\beta_2\epsilon_2}\right)^{-1} \prod_{\mu'} \left(1 + e^{\beta_{\mu'}\epsilon_{\mu'}}\right) \left[-1 + \cosh(\tau X) + \sinh(\tau X)\right]}, \tag{15}$$

where $X = \cosh(\beta_1\epsilon_1/2) + \cosh(\beta_2\epsilon_2/2)$. In a similar fashion, the system efficiency reads $\eta_s = 1 - \epsilon_1/\epsilon_2$, which is independent of fluxes and temperatures. Both of them can be related through expression $\mathcal{P}_s = -\epsilon_2 \eta_s \bar{J}_s$ consistent to heat engine characterized by $\bar{J}_s > 0$ (since $\beta_1\epsilon_1 > \beta_2\epsilon_2$), $\mathcal{P}_s < 0$, $0 \leq \eta_s \leq \eta_c$. Such results are in agreement with Refs. [25, 26, 56] for $\mu_1 = \mu_2 = 0$. Conversely, the pump is characterized by the other way around of conditions $\bar{J}_s < 0$ (since $\beta_1\epsilon_1 < \beta_2\epsilon_2$), $\mathcal{P}_s > 0$ and $\eta_c < \eta_s \leq 1$.

B. Main expressions and general findings

Transition rates $\omega_{ij}^{(\nu)}$ follow Eq. (9) and have been defined them according to the standard Kramers form [16, 55]:

$$\omega_{10}^{(\nu)} = 2\Gamma \exp\left\{\frac{-\beta_\nu}{2}(V_\nu + \epsilon_\nu)\right\}, \tag{16}$$

$$\omega_{01}^{(\nu)} = \Gamma \exp\left\{\frac{-\beta_\nu}{2}(-V_\nu - \epsilon_\nu)\right\}, \tag{17}$$

$$\omega_{21}^{(\nu)} = \Gamma \exp\left\{\frac{-\beta_\nu}{2}(-V_\nu + \epsilon_\nu)\right\}, \quad \text{and} \tag{18}$$

$$\omega_{12}^{(\nu)} = 2\Gamma \exp\left\{\frac{-\beta_\nu}{2}(V_\nu - \epsilon_\nu)\right\} \tag{19}$$

where V_ν, ϵ_ν assume distinct values at each stage and Γ expresses the coupling between the system and the reservoir. From Eq. (11), the average heat flux at each stage is given by

$$\begin{aligned} \overline{\mathcal{Q}}_1 &= -\left[\bar{J}_{01}^{(1)}(V_1 + \epsilon_1) + \bar{J}_{21}^{(1)}(V_1 - \epsilon_1)\right], \\ \overline{\mathcal{Q}}_2 &= \left[\bar{J}_{01}^{(1)}(V_2 + \epsilon_2) + \bar{J}_{21}^{(1)}(V_2 - \epsilon_2)\right], \end{aligned} \tag{20}$$

whose steady entropy production $\overline{\sigma}$ assumes the generic fluxes times forces form $\overline{\sigma} = J_1X_1 + J_2X_2$, where $J_1 = \bar{J}_{01}^{(1)}$ and $J_2 = \bar{J}_{21}^{(1)}$ with X_1 and X_2 given by

$$\begin{aligned} X_1 &= \frac{V_1 + \epsilon_1}{T_1} - \frac{V_2 + \epsilon_2}{T_2}, \\ X_2 &= \frac{V_1 - \epsilon_1}{T_1} - \frac{V_2 - \epsilon_2}{T_2}. \end{aligned} \tag{21}$$

Expressions for the power $\mathcal{P}$ and system efficiency η are given by

$$\mathcal{P} = (\epsilon_1 - \epsilon_2)(\bar{J}_{01}^{(1)} - \bar{J}_{21}^{(1)}) + (V_1 - V_2)(\bar{J}_{01}^{(1)} + \bar{J}_{21}^{(1)}), \tag{22}$$

and

$$\eta = -\frac{(\epsilon_1 - \epsilon_2)(\bar{J}_{01}^{(1)} - \bar{J}_{21}^{(1)}) + (V_1 - V_2)(\bar{J}_{01}^{(1)} + \bar{J}_{21}^{(1)})}{\epsilon_2(\bar{J}_{01}^{(1)} - \bar{J}_{21}^{(1)}) + V_2(\bar{J}_{01}^{(1)} + \bar{J}_{21}^{(1)})}, \tag{23}$$

respectively. We pause again to make a few comments. First, Eqs. (20)-(23) are general for the two-stage case, irrespective of the period, asymmetry and model parameters. Second, in the absence of interactions ($V_1 \to 0$ and $V_2 \to 0$), the system becomes equivalent to the interactionless setup investigated previously. Third, contrasting with the interactionless case, there are two independent fluxes, $\bar{J}_{01}^{(1)}$ and $\bar{J}_{21}^{(1)}$, revealing that the interaction between units gives rise to a much richer behavior than the single case [25]. Eqs. (20) and (22) impose some constraints on the operation regime. In particular, the heat engine occurs when both inequalities $(\epsilon_2 - \epsilon_1)(\bar{J}_{01}^{(1)} - \bar{J}_{21}^{(1)}) < (V_1 - V_2)(\bar{J}_{01}^{(1)} + \bar{J}_{21}^{(1)})$ and $\epsilon_2(\bar{J}_{21}^{(1)} - \bar{J}_{01}^{(1)}) > V_2(\bar{J}_{01}^{(1)} + \bar{J}_{21}^{(1)})$ are simultaneously satisfied, whereas the pump regime takes place for opposite inequalities. Fourth, our system will operate more efficiently than the interactionless case ($\eta > \eta_s$) if $(\epsilon_1 V_2 - \epsilon_2 V_1)(\bar{J}_{01}^{(1)} + \bar{J}_{21}^{(1)}) > 0$. The ideal regime operation yields when $\bar{J}_{01}^{(1)}, \bar{J}_{21}^{(1)} \to 0$. For ϵ_1/ϵ_2 or V_1/V_2 held fixed, $\eta = \eta_c$ when $\beta_2 V_2 = \beta_1 V_1$ and $\beta_2\epsilon_2 = \beta_1\epsilon_1$, respectively, whose efficiency is given by $\eta = 1 - V_1/V_2$, akin

to the interactionless expression. Conversely, maximum efficiencies $\eta_{ME} < \eta_c$ if the condition $\epsilon_1/\epsilon_2 = V_1/V_2 = \beta_2/\beta_1$ is not satisfied. Fifth and last, the occurrence of the pump regime implies at the following relation between parameters $(\beta_2\epsilon_2 - \beta_1\epsilon_1)(\bar{J}^{(1)}_{21} - \bar{J}^{(1)}_{01}) > (\beta_2 V_2 + \beta_1 V_1)(\bar{J}^{(1)}_{21} + \bar{J}^{(1)}_{01})$. Figs. 2, 3 and Appendix C illustrate all above general features.

C. System behavior and heat maps for equal switching times $\tau_1 = \tau/2$

Once introduced the main expressions, we are now in a position to depict the system behavior and main results. Parameters will be defined in such a way that $\beta_\nu V_\nu$ and $\beta_\nu \epsilon_\nu$ are dimensionless. For simplifying matters, $\beta_\nu V_\nu > 0$ and $\beta_\nu \epsilon_\nu > 0$ The analysis will be carried out for the following set of parameters: $\beta_1 = 10, \beta_2 = 1$, $\tau = 1$. In order to obtain a first insight into how the interaction between units influences the system performance, Fig. 2 depicts the system performance for $\epsilon_1/\epsilon_2 = 0.5$, in which the interactionless case operates as an engine with power and efficiency given by $\mathcal{P}_s = -0.1477$ and $\eta_s = 0.5$, respectively.

We highlight two remarkable changes coming from the interaction, under suitable choices of $V_1(V_2)$ at stages $\nu = 1(2)$. The former is a broad set of parameters, in which $\eta > \eta_s$ and $\mathcal{P} > \mathcal{P}_s$. The inclusion of interactions also extends the regime of operation, giving rise to a pump regime as V_2 goes up. Similar results are found for distinct β_1/β_2's, although the variation of temperatures can favor a given operation regime (see e.g. Appendix C). For such choice of parameters, maximum efficiency $\eta_{ME} < \eta_c$ and $\mathcal{P}_{mP}$ yield for negative values of V_1.

The interplay between individual ϵ_1/ϵ_2 and interaction V_1/V_2 energies is depicted in Fig. 3, in which $\eta < \eta_s < \eta_c$ for small V_2's. However, its increase not only extends the heat regime to the region $0 < \epsilon_1/\epsilon_2 < \beta_2/\beta_1$, in which the interactionless case operates as a pump, but also leads to higher efficiencies $\eta > \eta_s$ as V_2 increases and a maximum efficiency η_{ME} at V_{2ME}. As portrayed in Sec. III B, $\eta_{ME} < \eta_c$ for $\epsilon_1\beta_1 \neq \epsilon_2\beta_2$ and $\eta_{ME} = \eta_c$ at $V_2 = V_{2ME}$ when $\epsilon_1\beta_1 = \epsilon_2\beta_2$ (e.g. blue • in Fig. 3) and the interactionless case is efficient in such latter case. Similarly to η, it is possible to find suitable values of parameters in which $\mathcal{P} > \mathcal{P}_s$ (from now on meaning the absolute value of $\mathcal{P}$) as well as optimize it via a suitable choice of V_{2mP} providing the maximum power $\mathcal{P}_{mP}$. However, there is a remarkable difference with respect to η, the existence of an optimal set of ϵ_1/ϵ_2 and V_2 in which (the absolute) $\mathcal{P}$ is simultaneously maximized (see e.g. symbol $*$ in bottom heat maps).

The influence of V_1 (V_2 held fixed) is remarkably different from left panels (V_1 held fixed), and the engine regime and higher efficiencies are constrained to small values of V_1's (consistent with the general findings from Sec. III B), hence pointing us out that stronger interactions in the second stage are more significant than in the first one (second stage operating as the hot thermal bath). Also, $\eta > \eta_s$ for a broader set of values of V_1 as ϵ_1/ϵ_2 is large. The behavior of $\mathcal{P}$ is akin to the previous one and presents a maximum at a (small) V_{1mP}'s (fixed ϵ_1/ϵ_2) as well as an optimal ϵ_1/ϵ_2 providing its simultaneous maximization.

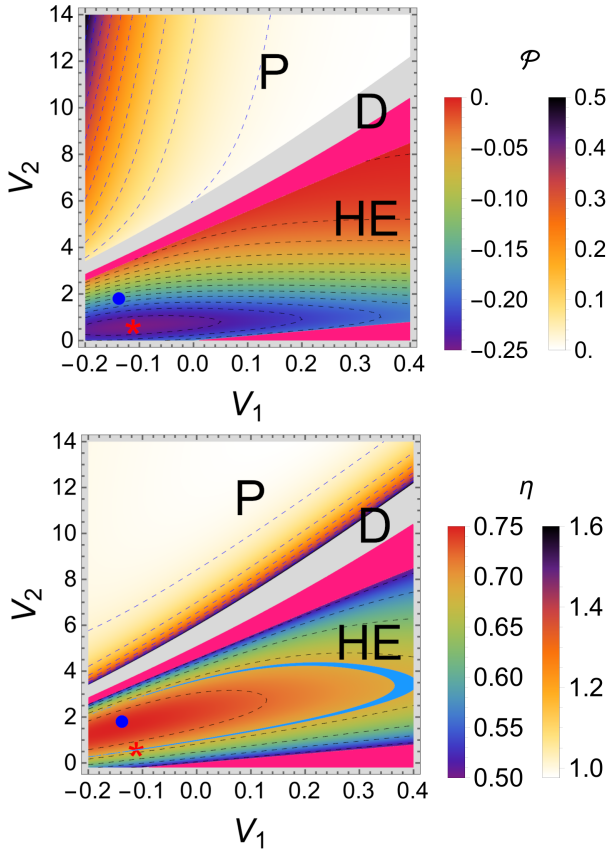

FIG. 2. The influence of the interaction parameters over the system performance. The top and bottom panels depict the power and efficiency heat maps. The surfaces highlighted by the color pink represent the region in which $\eta \leq \eta_s$. Parameters: $\beta_2 = 1, \beta_1 = 10, \tau = 1$ and $\epsilon_1/\epsilon_2 = 0.5$. Symbols HE (left bars) and P (right bars) correspond to the heat engine and pump regimes, respectively, whereas * and • show to the global maximum of $\mathcal{P}_{mP}$ and η_{ME} in the HE regime. The gray region indicates dud (D) behavior. For this set of parameters $\eta_{ME} < \eta_c$, whereas the light blue line in the bottom panel indicates the region in which $\eta_{mP} = \eta_{CA}$.

As a side analysis, we compare efficiencies at maximum power η_{mP} with Curzon and Ahlborn bound $\eta_{\rm CA}$ given by $\eta_{\rm CA} = 1 - \sqrt{\beta_2/\beta_1}$ [57], which has been verified in distinct systems [2, 17, 58]. Despite not constituting a universal result, it provides a powerful guide about the system operation at finite power, which is more realistic than the ideal case ($\eta = \eta_c$ and $\mathcal{P} = 0$). In all cases, the interaction among units can also be chosen for providing efficiencies at maximum power $\eta_{mP} > \eta_{CA}$ for a wide range of parameters (see e.g. light blue lines in Figs. 2-3 in which $\eta_{mP} = \eta_{CA}$). Depending on the parameters the engine is projected, $\eta_{mP} < \eta_{CA}$ [Figs. 2 and 3 (left panel)] and $\eta_{mP} > \eta_{CA}$ (right panel of Fig. 3) at the simultaneous maximization of power.

Summarizing our findings, the presence of collective effects between two units makes it possible to conveniently choose interaction parameters at each stage, providing higher performances than its interactionless counterpart (for the same

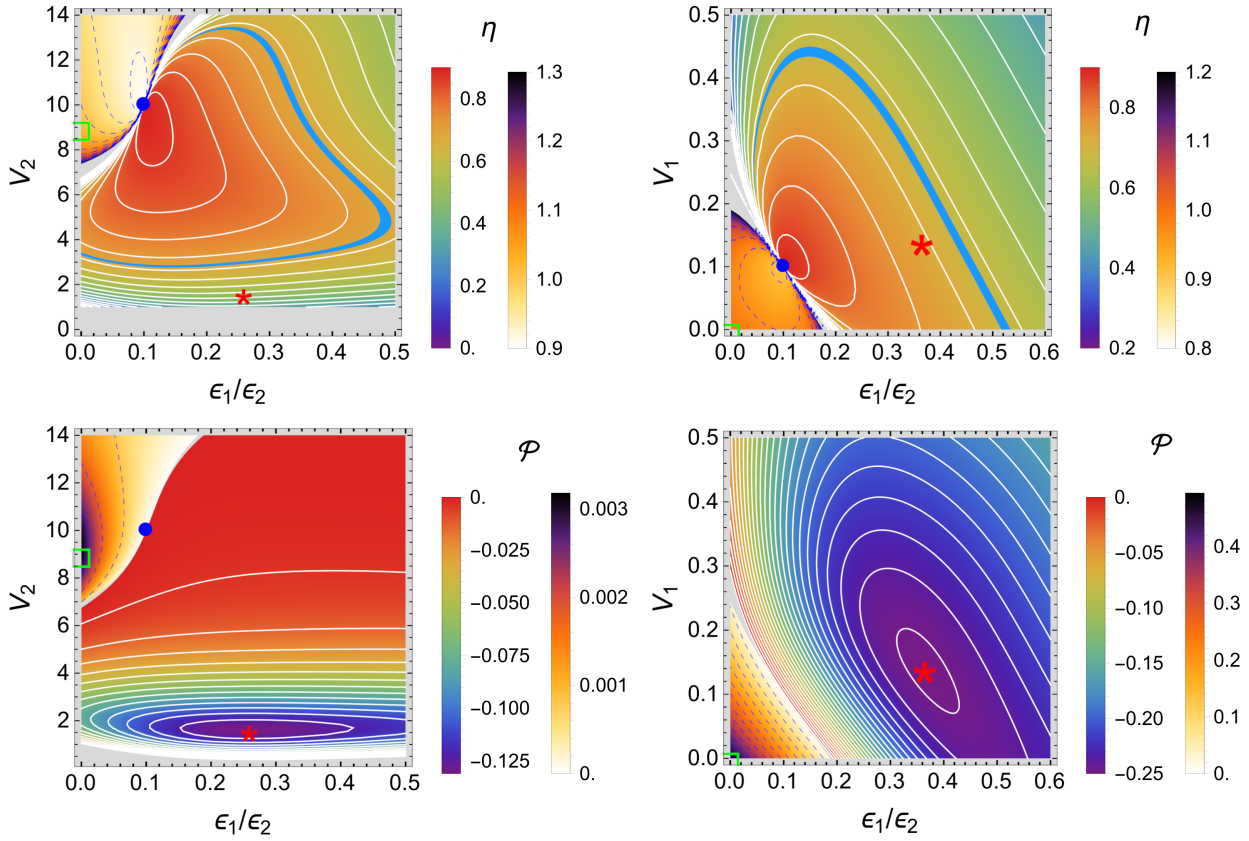

FIG. 3. The influence of individual energies ϵ_1/ϵ_2 over the system performance. Left and right panels depict fixed V_1 and V_2, respectively, while top and bottom panels show η's and $\mathcal{P}$'s heat maps, respectively. The left and right bars denote HE and P regimes, respectively. Symbols •, * and □ estimate the location of the Carnot efficiency η_c, efficiencies at maximum power η_{mP} at the heat engine (HE) and pump (P) regimes, respectively. Light blues in top panels indicate the regions in which $\eta_{mP} = \eta_{CA}$. Parameters: $\beta_2 = 1, \beta_1 = 10, \tau = 1$, $V_2 = 1$ (right) and $V_1 = 1$ (left).

values of individual energies), as well as distinct optimization routes, such as the maximization of power and efficiency. Additionally, an extra advantage concerns the possibility of changing the regime operation, from heat engine to pump and vice-versa, by changing the interactions at each stage.

D. Influence of period τ and asymmetric switchings

The influence of period τ and the inclusion of a different time duration at each stage, expressed by $\kappa = \tau_1/\tau_2 \neq 1$ will be considered in this section. Due to the existence of several distinct parameters, we shall focus on parameters $\epsilon_1/\epsilon_2 = 0.6$, $V_1 = 0.2, \beta_1 = 10$, and $\beta_2 = 1$.

Although $\mathcal{P}_s$ increases as τ is lowered, the period plays a less important role in the interactionless case, in part because η_s is independent of J_s and τ [25, 56]. On the other hand, the existence of two independent fluxes, as a consequence of the interaction between nanomachines makes the influence of τ more revealing. We highlight two aspects regarding the influence of τ, as depicted in the left panels of Fig. 4. First, it significantly affects the system performance, marking the increase of both $\mathcal{P}$ (as the interactionless system) and η (unlike the interactionless), with increasing maximum $\mathcal{P}_{mP}$ and η_{ME} at V_{2mP} and V_{2ME}, respectively, as τ is decreased toward the limit $\tau \to 0$, in which the system becomes equivalent to the (simultaneous) contact with hot and cold thermal baths (see e.g. Appendix B). Second, despite the increase of τ reduces $\mathcal{P}$ and η, it enlarges the heat engine operation. Thus, the period can be conveniently chosen to obtain a desirable compromise between the system performance (power and efficiency) and the range of the operation regime.

A second aspect to be investigated in this section relies on the inclusion of a distinct duration of each stage, measured by the asymmetry κ. This ingredient has been revealed to be a powerful ingredient for improving the system power in the interactionless case [28] or even both $\mathcal{P}$ and η in the case of collisional Brownian engines [23] and is depicted in the right panels of Fig. 4. Although η typically increases as V_2 raises and κ (or τ_1) is reduced, consistent with the system placed in contact with the hot thermal bath during a larger interval, there is an optimal κ_o ensuring optimal power $\mathcal{P}_{mP}$. Thus, like the interactionless case [28], κ can be conveniently chosen in order to increase the power-output and $\mathcal{P} > \mathcal{P}_s$. Since $\eta > \eta_s$ for a broad range of V_2's, the interaction offers an extra advantage in which κ can be suitably chosen in order to obtain

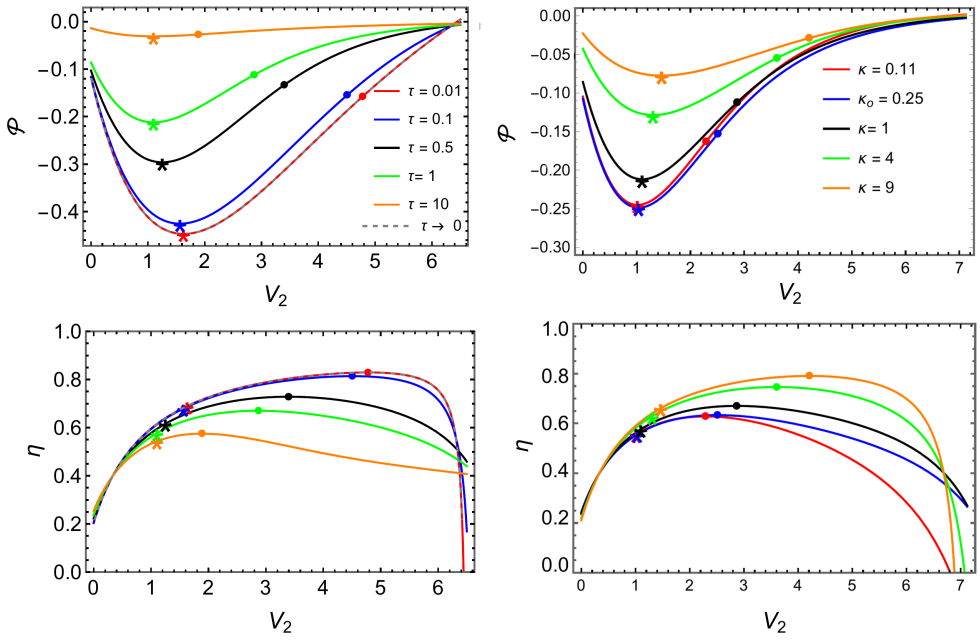

FIG. 4. Left and right panels depict the influence of period τ (for symmetric time switchings) and distinct κ's (for $\tau = 1$), respectively, for $\mathcal{P}$ (top) and η (bottom), respectively. The values of τ (left) and κ (right) decrease from top to bottom curves. Symbols $*$ and $\bullet$ denote associate $\mathcal{P}_{mP}$'s and η_{ME}'s, respectively. Parameters: $\beta_1 = 10, \beta_2 = 1, V_1 = 0.2, \epsilon_1/\epsilon_2 = 0.6$.

the desired η (greater than η_s) or even the desired compromise between $\mathcal{P}$ and η.

IV. COLLISIONAL MACHINE UNDER NON CONSERVATIVE DRIVINGS

A. Main expressions and heat maps

Our second approach encompasses a worksource coming from a non-conservative driving, introduced through a bias to benefit certain transitions. By following the ideas of Refs.[16, 17, 49], transitions of type $i \to i+1$ ($i \to i-1$) are favored according to whether the system is placed in contact with the cold (hot) thermal baths, through a biased driving force with strength F_ν, whereas the remaining parameters (V and ϵ) are held fixed. Our study relies on investigating two important aspects: the role of drivings at each stage and its relationship with V, temperatures β_1/β_2 and the influence of period τ. Transition rates $\omega_{ij}^{(\nu)}$ follow Eq. (9) and are listed below

$$\omega_{10}^{(\nu)} = 2\Gamma \exp\left\{\frac{-\beta_\nu}{2}(E_a + V + \epsilon + (-1)^\nu F_\nu)\right\} \quad (24)$$

$$\omega_{01}^{(\nu)} = \Gamma \exp\left\{\frac{-\beta_\nu}{2}(E_a - V - \epsilon - (-1)^\nu F_\nu)\right\} \quad (25)$$

$$\omega_{21}^{(\nu)} = \Gamma \exp\left\{\frac{-\beta_\nu}{2}(E_a + \epsilon - V + (-1)^\nu F_\nu)\right\} \quad (26)$$

$$\omega_{12}^{(\nu)} = 2\Gamma \exp\left\{\frac{-\beta_\nu}{2}(E_a - \epsilon + V - (-1)^\nu F_\nu)\right\}, \quad (27)$$

where F_ν assumes distinct values at each stage. Parameter E_a denotes an activation energy and it will be included in order to draw a comparison with previous results [15, 16]. Although our main findings are independent of E_a, its inclusion makes the heat engine regime more pronounced. From now on, we shall set $E_a = 1$ in all analyses.

From Eqs. (12) and (13) and by taking $V_1 = V_2 = V$ and $\epsilon_1 = \epsilon_2 = \epsilon$, the average power and the heat extracted exchanged with the hot bath is given by the following expressions

$$\begin{aligned} \mathcal{P} &= -(F_1 + F_2)(\bar{J}_{01}^{(1)} - \bar{J}_{21}^{(1)}), \\ \overline{\dot{Q}}_2 &= \left[(V + \epsilon + F_2)\bar{J}_{01}^{(1)} + (V - \epsilon - F_2)\,\bar{J}_{21}^{(1)}\right], \end{aligned} \quad (28)$$

whose system entropy production reads $\bar{\sigma} = -\beta_1\overline{\dot{Q}}_1 - \beta_2\overline{\dot{Q}}_2$ and assumes the bilinear form $\overline{\sigma} = J_1X_1 + J_2X_2$, where $J_1 = \bar{J}_{01}^{(1)}$ and $J_2 = \bar{J}_{21}^{(1)}$ (as in Sec. III) with thermodynamic forces X_1 and X_2 given by

$$\begin{aligned} X_1 &= \frac{\epsilon + V + F_2}{T_2} - \frac{\epsilon + V - F_1}{T_1}, \\ X_2 &= \frac{\epsilon - V + F_2}{T_2} - \frac{\epsilon - V - F_1}{T_1}. \end{aligned} \quad (29)$$

The efficiency is given by the ratio between $\mathcal{P}$ and $\overline{\dot{Q}}_2$ given by

$$\eta = \frac{(F_1 + F_2)(\bar{J}_{01}^{(1)} - \bar{J}_{21}^{(1)})}{(V + \epsilon + F_2)\bar{J}_{01}^{(1)} + (V - \epsilon - F_2)\,\bar{J}_{21}^{(1)}}, \quad (30)$$

respectively. The existence of the heat engine and pump regimes imposes some constraints in the fluxes, implying that in the former case, parameters have to be adjusted in such a

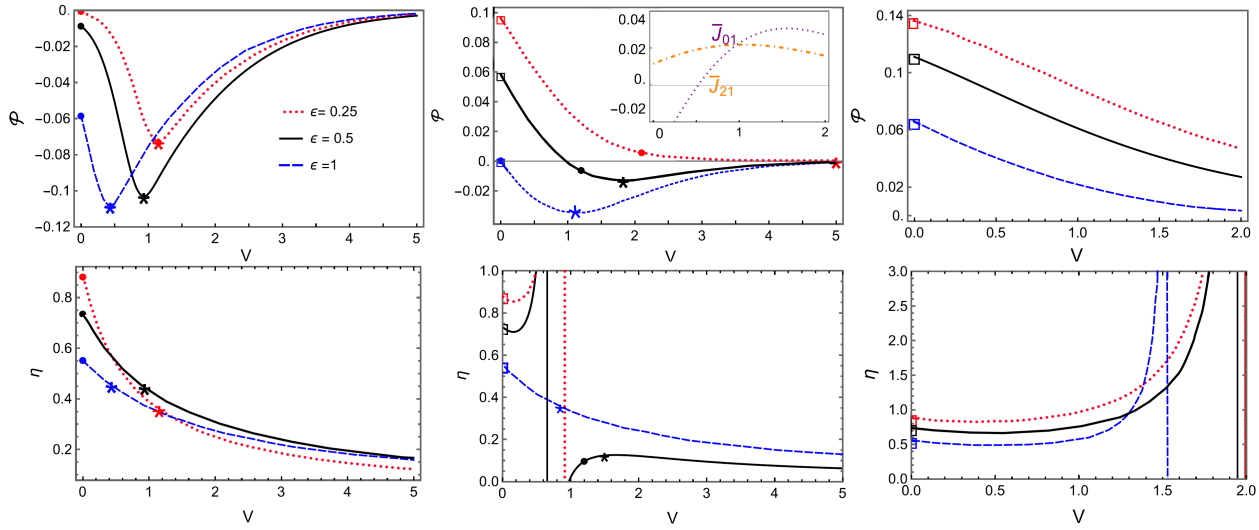

FIG. 5. Depiction of power $\mathcal{P}$ (top) and efficiency $\hat{\eta}$ (bottom) versus V for distinct β_1's. Parameters: $\beta_2 = 1, E_a = 1, F_2 = 1, F_1 = 0.1$ and $\tau = 1$ and $\beta_1 = 10$ (left), $\beta_1 = 20/9$ (middle) and $\beta_1 = 3/2$ (right). Stars and squares denote the location of $\mathcal{P}_{mP}$'s for heat engine and pump, respectively. Circles denote the location of maximum efficiencies for the engine ($0 \leq \eta < \eta_c$ regime.

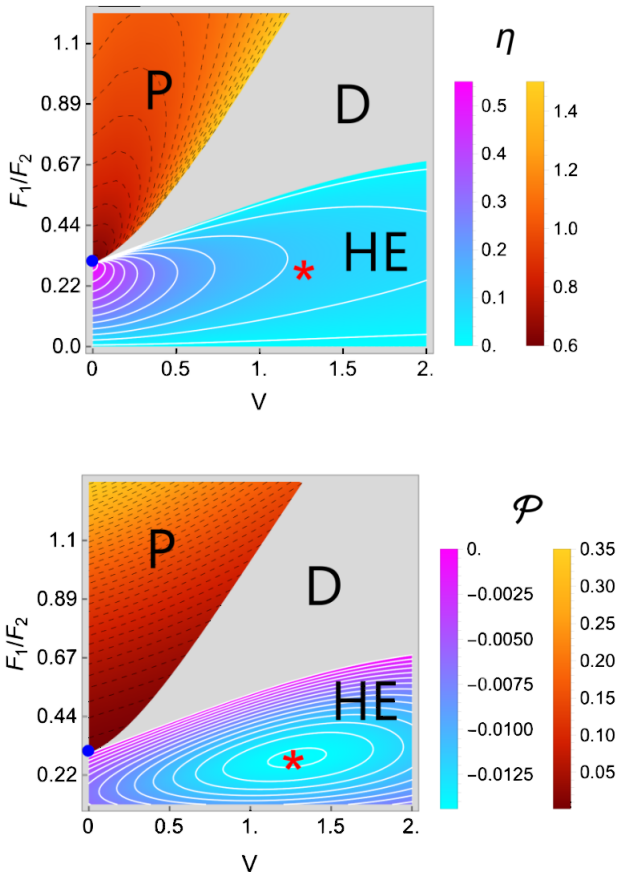

FIG. 6. Influence of nonconservative drivings and the interaction on the performance. Efficiency (top) and power (bottom) phase diagrams. Symbols P, D, and HE denote pump, dud, and heat engine regimes, respectively. Parameters: $\epsilon = 0.5, \beta_2 = 1, \beta_1 = 20/9, E_a = 1, \tau = 1, F_2 = 0.45$

way that $\bar{J}^{(1)}_{01} > \bar{J}^{(1)}_{21}$ and $V(\bar{J}^{(1)}_{01} + \bar{J}^{(1)}_{21}) > (\epsilon + F_2)(\bar{J}^{(1)}_{21} - \bar{J}^{(1)}_{01})$, whereas the latter (pump) implies opposite inequalities. A first insight about the influence of drivings is depicted in Figs. 5 for fixed F_1/F_2. Efficiency and power curves exhibit an interesting and rich behavior due to the interplay among parameters $\epsilon, V, \beta_1/\beta_2$ and τ. While the heat regime is levered by increasing ϵ and/or the ratio β_1/β_2 (left and middle panels), the pump regime is favored for lower values of β_1/β_2 (middle and right). The crossover from the heat to the pump regimes gives rise to an intermediate regime in which the system operates dudly (see e.g. middle panels). In such a case, there are optimal interactions V_{MP} and V_{ME}, marking maximum (absolute) power ($\mathcal{P}_{MP}$) and efficiency (η_{ME}), respectively. Conversely, only $\mathcal{P}$ can be optimized when the crossover between the above regimes is marked by the absence of a dud regime (e.g. left and right panels) and η monotonically decreases upon V being raised. Fig. 6 extends the above findings by depicting heat maps for the efficiency and power for distinct ratio F_1/F_2 and fixed ϵ. Similarly to systems composed of many interacting units under fixed drivings [15, 17] and results from Sec. III, the power $\mathcal{P}$ presents a simultaneous maximization (concerning both V and F_1/F_2), whereas η approaches to the ideal regime when F_2/F_1 is increased. However, a difference concerning previous studies concerns the absence of heat engine as $F_1 = F_2$. Unlike Refs. [15–17], in which the heat engine was investigated for large N's, our minimal setup of $N = 2$ interacting units requires a desirable compromise between F_ν's and parameters for operating properly as a heat engine.

The influence of period is depicted in Fig. 7 for the same parameters from Fig. 6 (left and right panels). In both cases, $\mathcal{P}$ is strongly influenced by the period and approaches to the simultaneous contact with baths as $\tau \to 0$, whose expressions are evaluated via Appendix B.

Also, depending on the parameters the engine is projected (right panels), the increase of τ changes the regime operation,

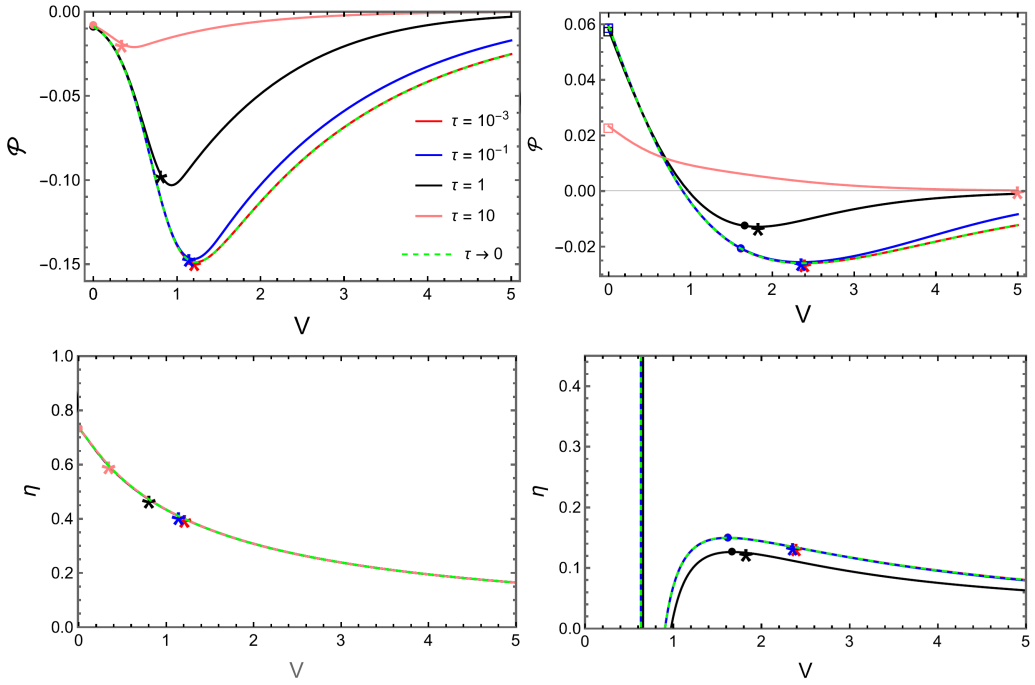

FIG. 7. The influence of period τ over the system performance. Depiction of $\mathcal{P}$ and η versus V for distinct τ's for $\beta_1 = 10$ (left) and $\beta_1 = 20/9$ (right). The values of τ increase from bottom to top curves (upper panels) and differences are almost imperceptible in the lower. Parameters: $\beta_2 = 1, E_a = 1, \epsilon = 0.5, F_2 = 1, F_1 = 0.1$.

from heat engine to pump. In both cases, the behavior of η is more revealing and mildly changes with τ. While small differences are almost imperceptible in the left panels, a somewhat increase of η as τ is lowered is verified. This finding is remarkable, because it may be used for conveniently choosing the period to obtain the desirable $\mathcal{P}$ with a small variation of η.

B. Asymmetric time switchings

In the last analysis, we investigate the influence of asymmetric interaction times in the presence of distinct drivings at each stage, as shown in Fig.8. In similarity with Fig. 4, the asymmetry can be conveniently chosen for enhancing the power and efficiency or even for obtaining a desirable compromise between them. There is an optimal κ_o leading to simultaneous maximization of power while η always increases as κ is lowered, consistent with the contact with a hot bath for a larger amount of the period. Despite such similarities, the asymmetry seems to be less pronounced than in the previous case, and optimal quantities do not deviate significantly from the symmetric ($\kappa = 1$) case. A possible reason is that power and efficiency exhibit a more intricate dependence on fluxes and changes of energy parameters (former approach) than on driving variations [see, *e.g.*, Eqs. (22)-(28) and (23)-(30)].

V. CONCLUSIONS

Nanoscopic engines operating via collective operation have attracted considerable attention and posed as potential candidates for the construction of reliable setups. However, given that most studies are restricted to fixed thermodynamic forces, little is known about how its construction influences the performance. The present study aimed to fill partially this gap by investigating the thermodynamic quantities of a minimalist collective model placed sequentially with distinct thermal baths at each stage. Distinct aspects have been addressed, such as different worksources, the role of interactions, the period, and the time durations of each stage. Results indicate that our minimal approach, together with a suitable choice of parameters, not only can boost the system performance, providing optimal power outputs and efficiencies greater than its interactionless case but also guide the operation regime, including distinct heat engine and pump regimes. Although the ideal regime $\tau \to 0$ provides higher performances than for finite τ's, the present contribution sheds light on how the interplay between interaction and individual parameters, together with a suitable tuning of the interaction time can optimize both power and efficiency as much as possible under more a realistic context (finite τ). Another remarkable finding concerns that the case of the system simultaneously placed in contact with two thermal reservoirs, previously investigated in various works [16, 21, 53], constitutes a particular case of our framework for fast switchings. As future extensions of our paper, it might be interesting to extend our sequential framework to setups composed of a larger number of nanomachines as well

as draw a comparison among their interactions.

VI. ACKNOWLEDGMENTS

This study was supported by the Special Research Fund (BOF) of Hasselt University under Grant No. BOF23BL14. We acknowledge the financial support from CAPES and FAPESP under grants 88887.816488/2023-00 and 2021/03372-2, respectively. The financial support from CNPq is also acknowledged.

Appendix A: Obtaining the exact solution for the boundary conditions

As described in the main text, by resorting to the eigendecomposition of the evolution matrix, together above boundary conditions, we arrive at the following expression f or the probability component $p_i^{(\nu)}(t)$ at the ν-th stage:

$$p_i^{(\nu)}(t) = p_i^{(eq,\nu)} + \sum_{j=1}^{2} e^{\lambda_j^{(\nu)}[t-(\nu-1)\frac{\tau}{2}]}\Gamma_j^{(\nu)}\mathbf{p}^{(\nu)}((\nu-1)\frac{\tau}{2}), \quad \text{(A1)}$$

where $\mathbf{p}^{(eq,\nu)}$ is the stationary state probability associated with $\lambda_0 = 0$ and $\lambda_j^{(\nu)}$ is the j-th non-zero eigenvalue and $\Gamma_j^{(\nu)} = \left|\psi_j^{(\nu)}\right\rangle\left\langle\phi_j^{(\nu)}\right|$ is the matrix associated with the product of the j-th right and left eigenvectors and $\mathbf{p}^{(\nu)}((\nu-1)\frac{\tau}{2})$ is the vector at each stage given by

$$\mathbf{p}^{(1)}(0) = \frac{-\left[e^{\tau W^{(1)}/2} + e^{\tau\left(\lambda_1^{(2)}+\lambda_2^{(2)}+\lambda_1^{(1)}+\lambda_2^{(1)}\right)/2}\right]\mathbf{p}^{(eq,1)} + \sum\limits_{\nu,\mu,\mu'} e^{\tau\left(\lambda_1^{(2)}+\lambda_2^{(2)}+\lambda_\nu^{(1)}\right)/2}\Delta_{\mu,\mu'}^{(1)}\left[\Gamma_{\mu'+1}^{(2)}\mathbf{p}^{(eq,1)} + e^{-\tau\lambda_{\mu'+1}^{(2)}/2}\mathbf{p}^{(eq,2)}\right]}{2\left[\left(e^{\tau\lambda_1^{(1)}/2} - e^{\tau\lambda_2^{(1)}/2}\right)\left(e^{\tau\lambda_1^{(2)}/2} - e^{\tau\lambda_2^{(2)}/2}\right)\mathrm{Tr}\left\{\Gamma_2^{(1)}\Gamma_2^{(2)}\right\} - \left(e^{\tau\left(\lambda_2^{(1)}+\lambda_1^{(2)}\right)/2} - 1\right)\left(e^{\tau\left(\lambda_1^{(1)}+\lambda_2^{(2)}\right)/2} - 1\right)\right]} \quad \text{(A2)}$$

$$\mathbf{p}^{(2)}\left(\frac{\tau}{2}\right) = \frac{-\left[e^{\tau W^{(1)}/2} + e^{\tau\left(\lambda_1^{(1)}+\lambda_2^{(1)}+\lambda_1^{(2)}+\lambda_2^{(2)}\right)/2}\right]\mathbf{p}^{(eq,2)} + \sum\limits_{\nu,\mu,\mu'} e^{\tau\left(\lambda_1^{(1)}+\lambda_2^{(1)}+\lambda_\nu^{(2)}\right)/2}\Delta_{\mu,\mu'}^{(2)}\left[\Gamma_{\mu'+1}^{(1)}\mathbf{p}^{(eq,2)} + e^{-\tau\lambda_{\mu'+1}^{(1)}/2}\mathbf{p}^{(eq,1)}\right]}{2\left[\left(e^{\tau\lambda_1^{(1)}/2} - e^{\tau\lambda_2^{(1)}/2}\right)\left(e^{\tau\lambda_1^{(2)}/2} - e^{\tau\lambda_2^{(2)}/2}\right)\mathrm{Tr}\left\{\Gamma_2^{(1)}\Gamma_2^{(2)}\right\} - \left(e^{\tau\left(\lambda_2^{(1)}+\lambda_1^{(2)}\right)/2} - 1\right)\left(e^{\tau\left(\lambda_1^{(1)}+\lambda_2^{(2)}\right)/2} - 1\right)\right]} \quad \text{(A3)}$$

where

$$\Delta_{\mu,\mu'}^{(\nu)} = \mathrm{Tr}\left\{\Gamma_\mu^{(\nu+1)}\Gamma_{\mu'}^{(\nu)}\right\} - \Gamma_\mu^{(\nu+1)}\Gamma_{\mu'}^{(\nu)}$$

Appendix B: The fast time switchings $\tau \to 0$ and the two reservoirs case

In the regime of fast switching dynamics, $\tau \to 0$, one gets the following expressions for fluxes

$$\lim_{\tau\to 0} \bar{J}_{01}^{(1)} = \frac{1}{2Z}\left(\omega_{01}^{(1)}\omega_{10}^{(2)} - \omega_{10}^{(1)}\omega_{01}^{(2)}\right)\left(\omega_{12}^{(1)} + \omega_{12}^{(2)}\right), \quad \text{(B1)}$$

and

$$\lim_{\tau\to 0} \bar{J}_{21}^{(1)} = \frac{1}{2Z}\left(\omega_{21}^{(1)}\omega_{12}^{(2)} - \omega_{12}^{(1)}\omega_{21}^{(2)}\right)\left(\omega_{10}^{(1)} + \omega_{10}^{(2)}\right), \quad \text{(B2)}$$

where $Z = \left(\omega_{01}^{(1)} + \omega_{01}^{(2)}\right)\left(\omega_{12}^{(1)} + \omega_{12}^{(2)}\right) + \left(\omega_{10}^{(1)} + \omega_{10}^{(2)}\right)\left(\omega_{12}^{(1)} + \omega_{12}^{(2)}\right) + \left(\omega_{10}^{(1)} + \omega_{10}^{(2)}\right)\left(\omega_{21}^{(1)} + \omega_{21}^{(2)}\right)$. The above expressions can be understood from the fact the system relaxes "infinitely fast" to its steady state at each stage, allowing to rewrite Eq.(2) in the following form $\dot{p}_i^{(\nu)}(t) = \sum_{j\neq i}\{\omega_{ji}^{(\nu)}p_i(t) - \omega_{ij}^{(\nu)}p_j(t)\}$, where $p_i(t) = p_i^{(1)}(t) + p_i^{(2)}(t)$. Thus, the total dynamics is described by $\dot{p}_i(t) = \sum_{j\neq i}\{\Omega_{ji}p_i(t) - \Omega_{ij}p_j(t)\}$, where $\Omega_{ij} = \omega_{ij}^{(1)} + \omega_{ij}^{(2)}$, which is equivalent to the simultaneous contact with both thermal reservoirs. A second way of understanding such a limit comes from the time integration of Eq. (2) over each stage by taking into account the boundary conditions from Eq. (3). In such cases, the steady state regime is given by the following relations $(\omega_{01}^{(1)} + \omega_{01}^{(2)})p_1 - (\omega_{10}^{(1)} + \omega_{10}^{(2)})p_0 = 0$ and $(\omega_{20}^{(1)}+\omega_{20}^{(2)})p_0+(\omega_{12}^{(1)}+\omega_{12}^{(2)})p_2-(\omega_{01}^{(1)}+\omega_{01}^{(2)}+\omega_{21}^{(1)}+\omega_{21}^{(2)})p_1 = 0$. By solving above system of linear equations, together with the condition $p_0 + p_1 + p_2 = 1$, one finds the following expressions for the probabilities:

$$p_0 = \frac{1}{Z}\left(\omega_{01}^{(1)} + \omega_{01}^{(2)}\right)\left(\omega_{12}^{(1)} + \omega_{12}^{(2)}\right), \quad \text{(B3)}$$

$$p_1 = \frac{1}{Z}\left(\omega_{10}^{(1)} + \omega_{10}^{(2)}\right)\left(\omega_{12}^{(1)} + \omega_{12}^{(2)}\right), \quad \text{(B4)}$$

$$p_2 = \frac{1}{Z}\left(\omega_{10}^{(1)} + \omega_{10}^{(2)}\right)\left(\omega_{21}^{(1)} + \omega_{21}^{(2)}\right). \quad \text{(B5)}$$

It is worth mentioning that p_i's can be alternatively obtained via the spanning tree method for a system of two interacting units. From p_i's, fluxes are promptly obtained, providing the same results as Eq. (B1) and (B2). Thermodynamic quantities are straightforwardly evaluated, whose main expressions for $\mathcal{P}$, $\overline{\dot{Q}_2}$ and η and have been shown along the main text.

We close this section by pointing out above expressions are general and hold valid in both Secs. III and IV when $\tau \to 0$.

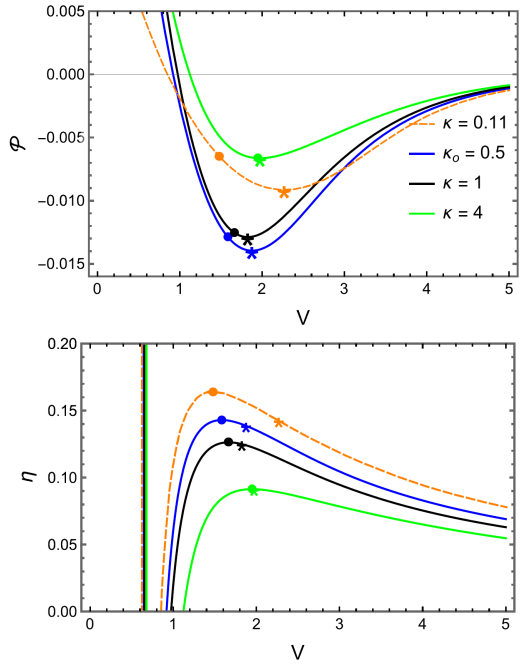

FIG. 8. Depiction of power $\mathcal{P}$ and efficiency η versus V for different κ. Symbols • and $*$ denote the maximization of efficiency and power, respectively. Except the dashed curve ($\kappa = 0.11$), the ratio κ decreases from top to bottom curves (upper panel) in the upper panel and increases in the lower one

. Parameters: $\epsilon = 0.5, \beta_2 = 1, \beta_1 = 20/9, E_a = 1, \tau = 1, F_1 = 0.1, F_2 = 1$.

Appendix C: Global phase diagram for distinct interactions at each stage

In this section, we depict the system phase diagram (top panel) built from inequalities, $(\epsilon_2 - \epsilon_1)(\bar{J}_{01}^{(1)} - \bar{J}_{21}^{(1)}) < (V_1 - V_2)(\bar{J}_{01}^{(1)} + \bar{J}_{21}^{(1)})$ and $\epsilon_2(\bar{J}_{21}^{(1)} - \bar{J}_{01}^{(1)}) > V_2(\bar{J}_{01}^{(1)} + \bar{J}_{21}^{(1)})$, shown in the main text for the heat engine (HE) regime and the other way around for the pump (P). In particular, the crossover between HE and P regimes will be characterized by ideal efficiency provided $\epsilon_1/\epsilon_2 = V_1/V_2 = \beta_2/\beta_1$ (green symbols). The bottom panels show, for different sets of temperatures, the phase diagram $V_1/V_2 \times \epsilon_1/\epsilon_2$. As discussed in the main text, while larger β_1/β_2 favors the HE regime, its decrease increases the region in which

[1] U. Seifert, Rep. Prog. Phys. **75**, 126001 (2012).
[2] C. Van den Broeck, Phys. Rev. Lett. **95**, 190602 (2005).
[3] H. B. Callen, *Thermodynamics and an Introduction to Thermostatistics*, 2nd ed. (Wiley, 1985).
[4] S. V. Moreira, P. Samuelsson, and P. P. Potts, Phys. Rev. Lett. **131**, 220405 (2023).
[5] J. H. Fritz, B. Nguyen, and U. Seifert, J. Chem. Phys. **152**, 235101 (2020).
[6] T. F. F. Santos, F. Tacchino, D. Gerace, M. Campisi, and M. F. Santos, Phys. Rev. A **103**, 062225 (2021).
[7] D. Zhao, (2021), arXiv:2112.12536 [physics.class-ph].
[8] R. Fu, O. M. Miangolarra, A. Taghvaei, Y. Chen, and T. T. Georgiou, Automatica **159** (2024).
[9] A. Kumari, M. Samsuzzaman, A. Saha, and S. Lahiri, Phys. A: Stat. Mech. Appl. **636** (2024).
[10] L. Peliti and S. Pigolotti, *Stochastic Thermodynamics: An Introduction* (Princeton University Press, 2021).
[11] H. Ge, M. Qian, and H. Qian, Phys. Rep. **510**, 87 (2012).
[12] S. Liepelt and R. Lipowsky, Phys. Rev. Lett. **98**, 258102 (2007).
[13] S. Liepelt and R. Lipowsky, Phys. Rev. E **79**, 011917 (2009).
[14] D. M. Busiello and C. E. Fiore, J. Phys. A: Math. Theor **55**, 485004 (2022).
[15] I. N. Mamede, K. Proesmans, and C. E. Fiore, Phys. Rev. Res. **5**, 043278 (2023).
[16] H. Vroylandt, M. Esposito, and G. Verley, EPL (Europhysics Letters) **120**, 30009 (2017).
[17] F. S. Filho, G. A. L. Forão, D. M. Busiello, B. Cleuren, and C. E. Fiore, Phys. Rev. Res. **5**, 043067 (2023).
[18] K. Proesmans, C. Driesen, B. Cleuren, and C. Van den Broeck, Phys. Rev. E **92** (2015).
[19] K. Proesmans, Y. Dreher, M. Gavrilov, J. Bechhoefer, and C. Van den Broeck, Phys. Rev. X **6** (2016).
[20] K. Proesmans and C. Van den Broeck, Chaos **27** (2017).
[21] I. N. Mamede, P. E. Harunari, B. A. N. Akasaki, K. Proesmans, and C. E. Fiore, Phys. Rev. E **105**, 024106 (2022).
[22] A. L. L. Stable, C. E. F. Noa, W. G. C. Oropesa, and C. E. Fiore, Phys. Rev. Res. **2**, 043016 (2020).
[23] C. E. F. Noa, A. L. L. Stable, W. G. C. Oropesa, A. Rosas, and C. E. Fiore, Phys. Rev. Res. **3**, 043152 (2021).
[24] I. N. Mamede, A. L. L. Stable, and C. E. Fiore, Phys. Rev. E **106**, 064125 (2022).
[25] A. Rosas, C. Van den Broeck, and K. Lindenberg, Phys. Rev. E **96**, 052135 (2017).
[26] A. Rosas, C. Van den Broeck, and K. Lindenberg, Phys. Rev. E **97**, 062103 (2018).
[27] S. Ray and A. C. Barato, Phys. Rev. E **96**, 052120 (2017).
[28] P. E. Harunari, F. S. Filho, C. E. Fiore, and A. Rosas, Phys. Rev. Res. **3**, 023194 (2021).
[29] V. Mukherjee and U. Divakaran, Journal of Physics: Condensed Matter **33**, 454001 (2021).
[30] W. Niedenzu and G. Kurizki, New Journal of Physics **20**, 113038 (2018).

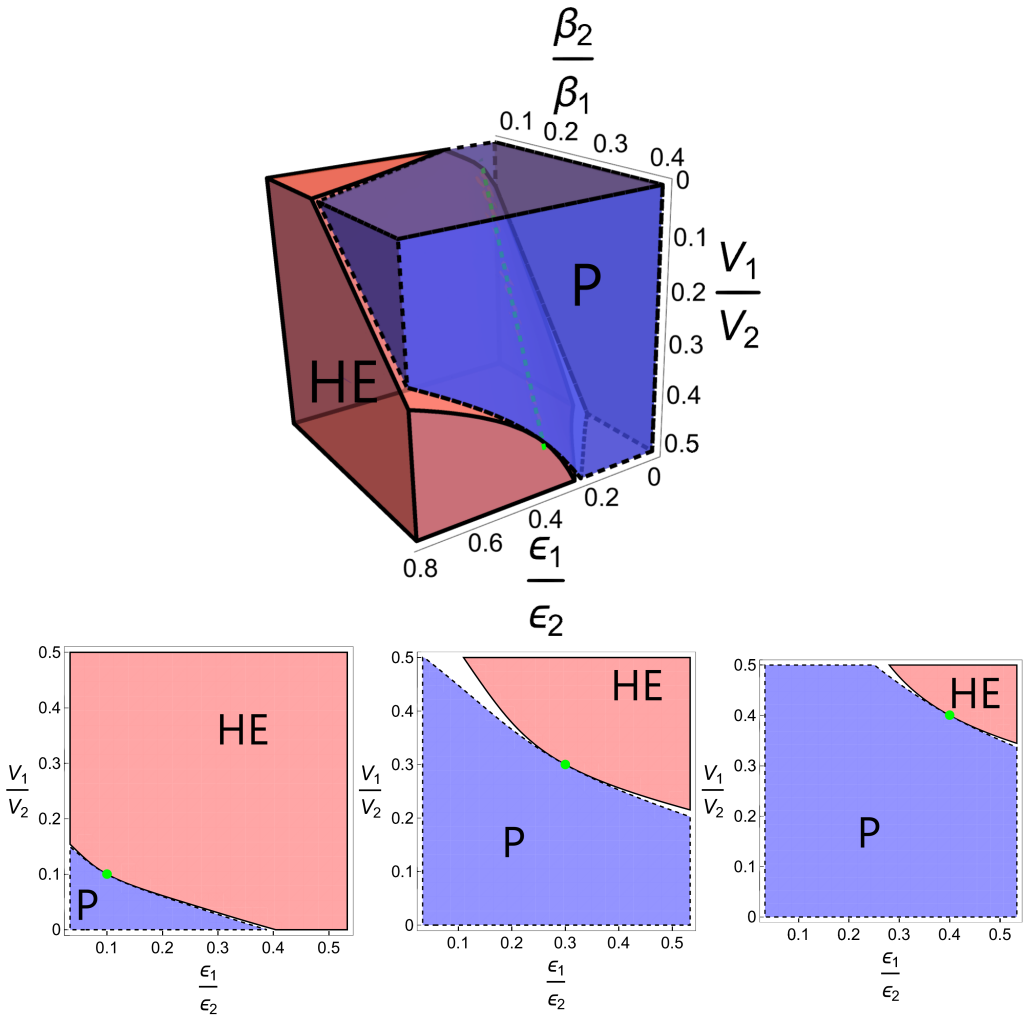

FIG. 9. Top panel: The phase diagram $\beta_2/\beta_1 \times V_1/V_2 \times \epsilon_1/\epsilon_2$. The green line represents the points where $\beta_2/\beta_1 = V_1/V_2 = \epsilon_1/\epsilon_2$. Bottom panels depict, for $\beta_1 = 10$ (left), $\beta_1 = 10/3$ (middle) and $\beta_1 = 10/4$ (right), the phase diagrams in the $V_1/V_2 \times \epsilon_1/\epsilon_2$ plane. P and HE denote, respectively, the pump and heat engine regimes. The white region shows the dud regime, whereas green bullets correspond to the ideal efficiency η_c.

[31] D. Kolisnyk and G. Schaller, Phys. Rev. Appl. **19**, 034023 (2023).
[32] C. L. Latune, I. Sinayskiy, and F. Petruccione, New Journal of Physics **22**, 083049 (2020).
[33] S. Kamimura, H. Hakoshimam, Y. Matsuzaki, K. Yoshida, and Y. Tokura, Physical Review Letters **128**, 180602 (2022).
[34] M. Macovei, A., Physical Review A **105**, 043708 (2022).
[35] C. H. Bennett, Int J Theor Phys **21**, 905 (1982).
[36] T. Sagawa, J. Stat. Mech.: Theory Exp. **2014**, P03025 (2014).
[37] V. Giovannetti and G. M. Palma, Phys. Rev. Lett. **108**, 040401 (2012).
[38] C. L. Latune, I. Sinayskiy, and F. Petruccione, Phys. Rev. Res. **1**, 033192 (2019).
[39] H. Ali and M. Özgür, E, Physical Review A **5**, 12953 (2015).
[40] N. Myers, F. J., O. Negrete, P. Vargas, G. De Chiara, and S. Deffner, New Jornal of Physics **24**, 025001 (2022).
[41] J. J., B. M., and C. A., del, New Jornal of Physics **18**, 075019 (2016).
[42] Y.-Y. Chen, G. Watanabe, Y.-C. Yu, X.-W. Guan, and A. del Campo, Nature Quantum Information **5**, 88 (2019).
[43] N. M., Myers and S. Deffner, Physical Review E **101**, 012110 (2020).
[44] M. Nathan, M., M. Jacob, and D. Sebastian, MDPI Symmetry **13**, 978 (2021).
[45] T. Fogarty and T. Busch, New Jornal of Physics **6**, 1 (2020).
[46] J. Li, T. Fogarty, S. Campbell, X. Chen, and T. Busch, New Journal of Physics **20**, 015005 (2018).
[47] T. Keller, T. Fogarty, J. Li, and T. Busch, Physical Review Research **2**, 033335 (2020).
[48] G. Watanabe, P. Venkatesh, B., P. Talkner, M.-J. Hwang, and A. del Campo, Phisical Review Letter **124**, 210603 (2020).
[49] T. Herpich, J. Thingna, and M. Esposito, Phys. Rev. X **8**, 031056 (2018).
[50] T. Herpich and M. Esposito, Phys. Rev. E **99**, 022135 (2019).
[51] L. P. Bettmann, M. J. Kewming, and J. Goold, Phys. Rev. E **107**, 044102 (2023).
[52] K. Prech, P. Johansson, E. Nyholm, G. T. Landi, C. Verdozzi, P. Samuelsson, and P. P. Potts, Phys. Rev. Res. **5**, 023155 (2023).

[53] H. Vroylandt, K. Proesmans, and T. R. Gingrich, J. Stat. Phys. **178**, 1039–1053 (2020).
[54] K. Proesmans and C. E. Fiore, Phys. Rev. E **100**, 022141 (2019).
[55] T. Tomé and M. J. de Oliveira, Phys. Rev. E **91**, 042140 (2015).
[56] F. Filho, B. Akasaki, C. Noa, B. Cleuren, and C. Fiore, Phys. Rev. E **106** (2022).
[57] F. L. Curzon and B. Ahlborn, Am. J. Phys. **43**, 22 (1975).
[58] I. Novikov, J. Nucl. Energy II **7**, 125 (1958).